



<b>Publication Year</b>	2015
<b>Acceptance in OA</b>	2020-03-23T16:04:06Z
<b>Title</b>	Spectral and timing characterization of the X-ray source 1RXS J194211.9+255552
<b>Authors</b>	D'AI, ANTONINO, CUSUMANO, GIANCARLO, LA PAROLA, VALENTINA, SEGRETO, ALBERTO
<b>Publisher's version (DOI)</b>	10.1093/mnras/stv1118
<b>Handle</b>	<a href="http://hdl.handle.net/20.500.12386/23471">http://hdl.handle.net/20.500.12386/23471</a>
<b>Journal</b>	MONTHLY NOTICES OF THE ROYAL ASTRONOMICAL SOCIETY
<b>Volume</b>	451

# Spectral and timing characterization of the X-ray source 1RXS J194211.9+255552

A. D’Aì,<sup>★</sup> G. Cusumano, V. La Parola and A. Segreto

INAF Istituto di Astrofisica Spaziale e Fisica Cosmica, Via U. La Malfa 153, I-90146 Palermo, Italy

Accepted 2015 May 13. Received 2015 May 2; in original form 2015 March 6

## ABSTRACT

We report on the first spectral and timing characterization of the transient X-ray source 1RXS J194211.9+255552 using all available data from the *Swift* X-ray satellite. We used 10 years of hard X-ray data from the Burst Alert Telescope (BAT) to characterize its long-term behaviour and to search for long periodicities, finding evidence for a periodic modulation at  $166.5 \pm 0.5$  d, that we interpret as the orbital period of the source. The folded light curve reveals that the X-ray emission is mostly concentrated in a restricted phase-interval and we propose to associate 1RXS J194211.9+255552 to the class of the Be X-ray binaries. This is also supported by the results of the spectral analysis, where we used the BAT data and three pointed *Swift*/XRT observations to characterize the X-ray broad-band spectral shape. We found mild spectral variability in soft X-rays that can be accounted for by a varying local neutral absorber, while the intrinsic emission is consistent with a hard power law multiplied by a high-energy exponential cut-off as typically observed in this class of systems.

**Key words:** X-rays: binaries – X-rays: individual: 1RXS J194211.9+255552.

## 1 INTRODUCTION

The X-ray source 1RXS J194211.9+255552 (J194211 hereafter) was first reported in the *ROSAT* All-Sky Faint Source Catalogue,<sup>1</sup> at RA = 295.549 59 and Dec. = 25.931 25 with a positional uncertainty of 18 arcsec and at a flux level of  $(1.8 \pm 0.7) \times 10^{-13}$  erg cm<sup>-2</sup> s<sup>-1</sup>. Probably due to its relative faintness, the source has been thereafter poorly studied. At the end of 2011 December, J194211 was clearly detected during the *INTEGRAL* Galactic Plane Scanning in soft X-rays at  $26 \pm 7$  mCrab (Chenevez et al. 2011). A follow-up observation with *Swift* allowed for the first determination of the X-ray spectrum, consistent with an absorbed (Galactic equivalent absorption column  $1.3 \pm 0.6 \times 10^{22}$  cm<sup>-2</sup>) power law of photon index  $\Gamma = 0.64$  and an unabsorbed flux in the 1–10 keV range of  $7.88 \times 10^{-11}$  erg cm<sup>-2</sup> s<sup>-1</sup> (Sidoli et al. 2011). The source positional error lead to the identification of two possible near-infrared counterparts, and Sidoli et al. (2011) proposed the association with the brighter one, the 2MASS star 19421116+2556056, whose optical spectrum (1159-0412038 in the USNO-B1.0 catalogue) is consistent with an early-type star (Masetti et al. 2012) pointing to the possible high-mass X-ray binary nature of the X-ray source.

We present here the first complete spectral and timing study in the X-ray domain of this source using all available data collected by the X-Ray Telescope (XRT) and Burst Alert Telescope (BAT) instruments on board of the *Swift* satellite.

## 2 DATA REDUCTION

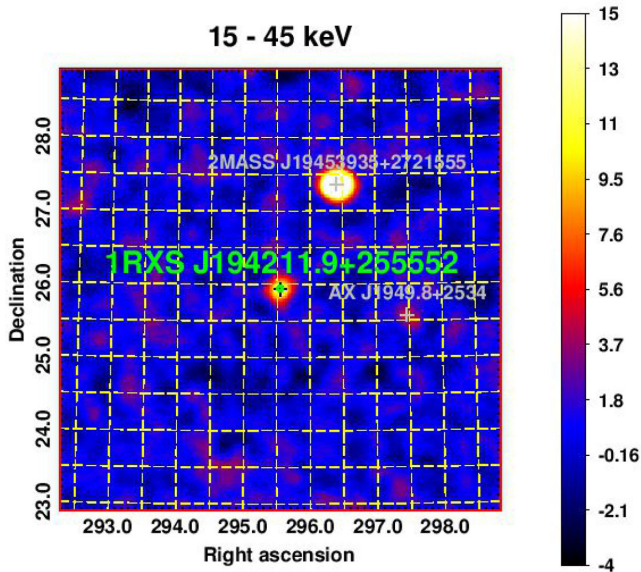
The survey data collected with *Swift*/BAT between 2004 December and 2014 June were retrieved from the HEASARC public archive<sup>2</sup> and processed using a software dedicated to the analysis of the data from coded mask telescopes (Segreto et al. 2010). The source is detected with a significance of 5.8 standard deviations in the 15–150 keV energy band, but the signal is optimized in the 15–45 keV energy band where we obtained a significance of 7.0 standard deviations.

Fig. 1 shows the significance map of the BAT sky region around J194211 in this energy band. We extracted a background subtracted light curve in the 15–45 keV band, binned at 15-d resolution to check the long-term source variability in hard X-rays (Fig. 2). The light curve clearly shows two different flux levels, with a significant higher flux in the more recent years. To have an estimate of the time when this enhanced activity began, we built the source signal-to-noise ratio (SNR) as a function of time; we started calculating the source significance using the entire 10-yr time-span; we then progressively removed one week of data from the start of the BAT monitoring and obtained the plot of the source significance as a function of the time window. We obtained the highest significance using the time window from 2010.6 to 2014.5 (magenta box in Fig. 2). The average BAT rate before 2010.6 has only an upper limit of  $3.6 \times 10^{-6}$  counts s<sup>-1</sup> pixel<sup>-1</sup>, that is

<sup>★</sup> E-mail: antonino.dai@ifc.inaf.it

<sup>1</sup> <http://www.xray.mpe.mpg.de/rosat/survey/rass-fsc/>

<sup>2</sup> <http://heasarc.gsfc.nasa.gov/docs/archive.html>



**Figure 1.** 15–45 keV *Swift*/BAT significance map centred on 1RXS J194211.9+255552.

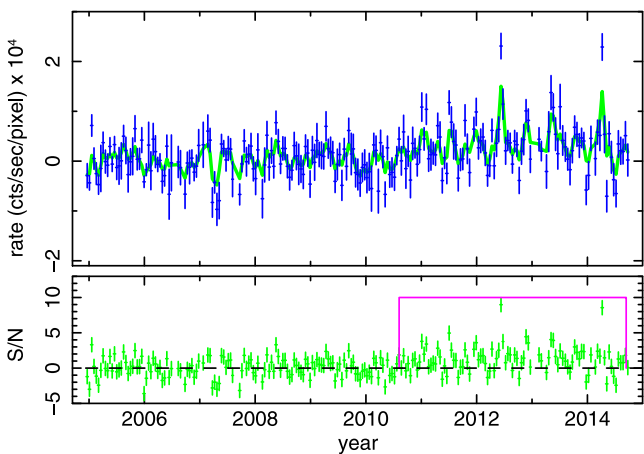


**Figure 2.** Long-term 15–45 keV *Swift*/BAT light curve (upper panel) and SNR (lower panel). Bin-time is 15 d. Magenta box indicates the time window of the active X-ray state.

compatible with zero, whereas in the period 2010.6–2014.5 the average rate increases to  $(3.3 \pm 0.4) \times 10^{-5}$  counts  $s^{-1}$  pixel $^{-1}$ .

During this active X-ray state, the light curve suggested a pattern of recurrent peaks (smoothed interpolated green line in Fig. 2), that we investigated performing a temporal analysis on the data (see Section 3).

J194221 was observed during three visits (Obs.ID 00032228001/02/03) with *Swift*/XRT in Photon Counting mode at the end of 2011 December, for a total collecting time of 6455 s. In Table 1, we show the log containing the details about the three *Swift*/XRT pointings.

The *Swift*/XRT data were processed using the *FTOOLS* package with standard procedures (*XRTPIPELINE* v.0.12.4), filtering and screening criteria, with standard grade filtering 0–12. The source is clearly detected in the three visits and no other contaminating source is present in the *Swift*/XRT field of view (see the left-hand panel of Fig. 1). To better constrain the source position, we stacked the three images and we obtained a refined source position at

RA = 19:42:11.22 and Dec. = +25:56:05.2 (1.9 arcsec error at 90 per cent confidence level) using the online *Swift*/XRT build products tool,<sup>3</sup> that allows also astrometric and enhanced position determination (Goad et al. 2007; Evans et al. 2014). This new position and error results are consistent with early estimates (Sidoli et al. 2011), but the smaller uncertainty allows us to better support the association of the possible infrared counterpart with the 2MASS object 19421116+2556056, as shown in Fig. 3.

A first inspection of the light curves showed mild variability, with averaged count rates per snapshot varying up to a factor of 2. The maximum count rate is  $\sim 0.53$  counts  $s^{-1}$  in Obs.ID 00032228001, close to the threshold indicated for a pile-up check.<sup>4</sup> We verified according to the suggested pipeline<sup>5</sup> that for this Obs.ID a circular region with 4 pixels radius (centred at the source position) must be excluded to avoid spectral pile-up distortions. Therefore, the source spectrum was extracted from an annular region of 4 and 40 pixels internal and external radius, respectively, centred on the source coordinates as previously determined. A background spectrum was extracted from an annular region of inner and outer radius 90 and 150 pixels, respectively. No pile-up correction was found necessary for the other two Obs.ID, and we used a circular region of 40 pixels radius to extract the source spectrum and the same annular region for the background spectrum.

The XRT ancillary response file generated with *XRTMKARF* accounts for PSF and vignetting correction; we used the spectral redistribution matrix v013 available in the *Swift* calibration data base. The spectral analysis was performed using *XSPEC* v.12.5, after grouping the spectrum with a minimum of 20 counts per channel to allow the use of  $\chi^2$  statistics. The source events arrival times were corrected to the SSB using the task *BARYCORR*.<sup>6</sup>

### 3 TIMING ANALYSIS

We performed a timing analysis of the *Swift*/BAT data searching for long-term periodic modulations in the 15–45 keV energy range during the enhanced activity period from 2010.6 to 2014.5. We applied a folding algorithm to the barycentred arrival times searching in the 1–1000 d time range with a step of  $P^2/(N \Delta T)$ , where  $P$  is the trial period,  $N = 16$  is the number of profile phase bins and  $\Delta T = 124$  Ms is the data time span. The average rate in each phase bin was evaluated by weighting the rates by the inverse square of the corresponding statistical errors (see Cusumano et al. 2010).

Fig. 4 (a) shows the periodogram with several features emerging. The most prominent one is at  $P_0 = 166.5 \pm 0.5$  d ( $\chi^2 = 172$ ), where the period and its error  $\Delta P_0$  are the centroid of the peak and the standard deviation obtained from a Gaussian fit to the  $\chi^2$  feature at  $P_0$ ; other significant features at higher (lower) periods corresponding to multiples (sub-multiples) of  $P_0$  are also clearly detected in the periodogram.

The long-term variability of the source causes the distribution of  $\chi^2$  to deviate sharply both in average and in fluctuation amplitude from the behaviour expected for a white noise signal dominated by statistical variations. As a consequence the  $\chi^2$  statistics cannot be applied, and for an estimation of the significance of this feature, we applied the following procedure (e.g. see also D’Aì et al. 2011).

<sup>3</sup> [http://www.swift.ac.uk/user\\_objects/](http://www.swift.ac.uk/user_objects/)

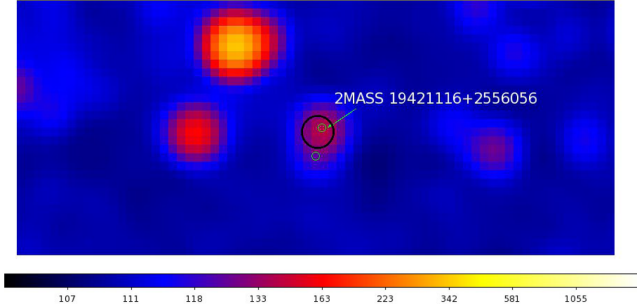
<sup>4</sup> see e.g. <http://www.swift.ac.uk/analysis/xrt/pileup.php>

<sup>5</sup> <http://www.swift.ac.uk/analysis/xrt/pileup.php>

<sup>6</sup> <http://heasarc.gsfc.nasa.gov/ftools/caldb/help/barycorr.html>

**Table 1.** Log of the pointed *Swift*/XRT observations of IRXS J194211.9+255552.

Obs.ID	Tstart UTC	Tstop UTC	Exposure (s)	Rate (counts s <sup>-1</sup> )
00032228001	2011-12-21 06:09:04	2011-12-21 07:37:02	1955	0.5261
00032228002	2011-12-24 04:40:04	2011-12-24 08:03:56	2063	0.4602
00032228003	2011-12-26 00:03:19	2011-12-26 03:25:57	2437	0.2641


**Figure 3.** 2MASS sky region around J194221. Black circle: our refined *Swift*/XRT position. Green circles: the two proposed infrared counterparts as reported in Sidoli et al. (2011).

(i) We fitted the periodogram between 50 and 250 d (characterized by a noise level consistent with the noise level at  $P_0$ ), excluding opportune intervals around the peaked features, with a linear fit that describes well the trend of the  $\chi^2$  values. The best-fitting function was then subtracted from the  $\chi^2$  to obtain a new flattened periodogram (hereafter,  $z$ ); the new  $z$  value at  $P_0$  is 148.2.

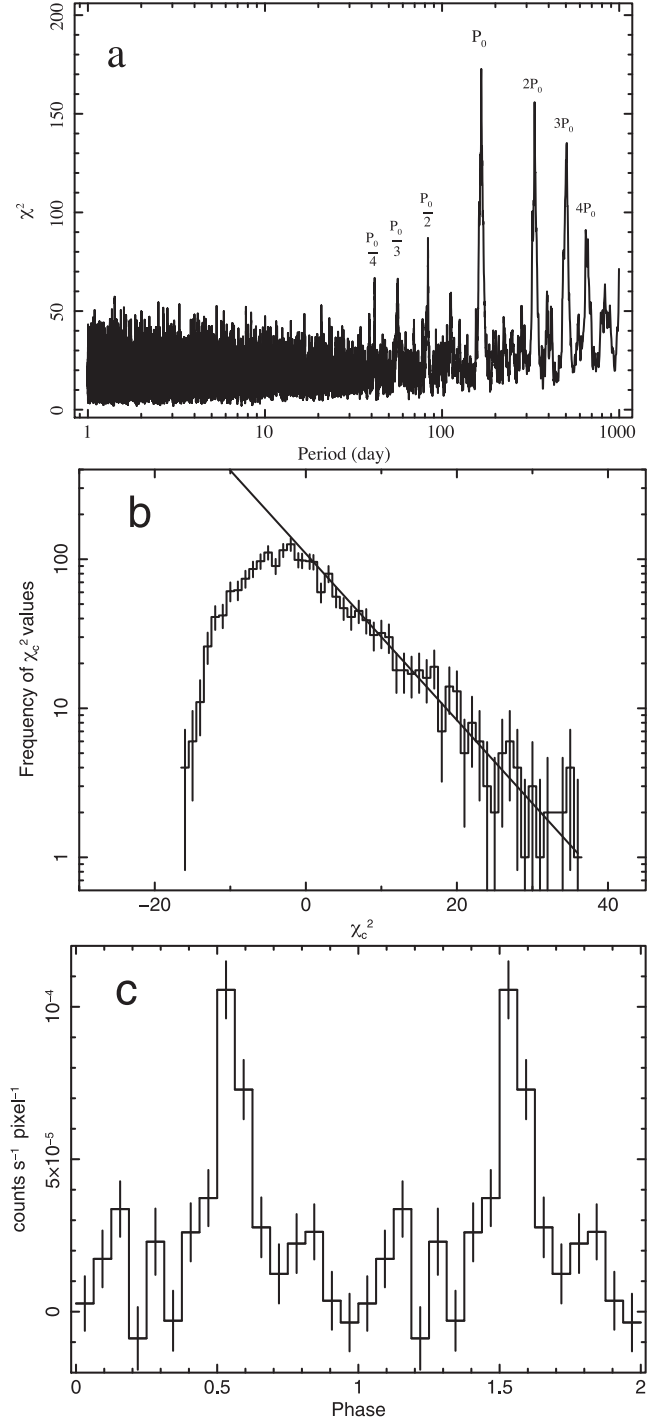
(ii) We then built the histogram of these  $z$  values, and fitted the positive tail of the histogram distribution (beyond  $z = 10$ ) with an exponential function, and we evaluated the integral,  $\Sigma$ , between 148.2 and infinity (normalized to the total area below the distribution). The area below the histogram was evaluated summing the contribution of each single bin from its left boundary up to  $z = 10$  and integrating the best-fitting exponential function beyond  $z = 10$ .  $\Sigma$  represents the probability of chance occurrence of  $z$  greater than 148.2.

iii) From the probability of chance occurrence ( $2.2 \times 10^{-9}$ ), we evaluated the corresponding significance of the feature at  $P_0$  in units of Gaussian standard deviations ( $\sim 6.0 \sigma$ ). The light-curve profile (Fig. 4, panel c) folded at  $P_0$  with  $T_{\text{epoch}} = 55828.91015625$  MJD is characterized by a peak of intensity  $\sim 4$  times higher than the profile-averaged flux and by a phase-span of  $\sim 1/8$  of the total period, corresponding to a duration of  $\sim 20$  d.

The three *Swift*/XRT observations fall at phases 0.524, 0.543, and 0.553 and, according to the folded profile, are in phase with the emission peak. We also searched for the presence of shorter periodic signals in the *Swift*/XRT data, performing a timing analysis on the arrival time of the source events extracted from each of the three *Swift*/XRT observations. In order to avoid systematics caused by the read-out time in PC mode (characterized by a time resolution bin of  $\delta T_{\text{XRT}} = 2.5073$  s), these arrival times were first randomized within  $\delta T_{\text{XRT}}$ . Then we performed a folding search in the range  $[\delta T_{\text{XRT}} : 500]$  s, but no significant feature above the level of noise was detected.

#### 4 SPECTRAL ANALYSIS

We studied the high-energy BAT spectrum collecting the events only after 2010.6 to optimize the SNR, but keeping all the available band


**Figure 4.** (a) Periodogram of *Swift*/BAT (15–45 keV) data for J194221. (b) Distribution of the  $z$  values derived from the  $\chi^2$  periodogram. The positive tail beyond  $z=10$  is modelled with an exponential function. (c) Light curve folded at a period  $P_0=166.5$  d, with 16 phase bins.

(15–150 keV energy range) to better constrain the cut-off energy of the spectrum. We produced a phase-averaged and a phase-selected spectrum in the phase-interval 0.3–0.7 that corresponds to the peak of the folded profile of Fig. 4. Both spectra were accumulated in eight energy channels and analysed using the BAT redistribution matrix available in the *Swift* calibration data base.<sup>7</sup> We fitted together the two spectra with a simple power law, and we obtained a satisfactory fit ( $\chi^2/\text{dof} = 15/14$ ) with a common photon index ( $\Gamma = 3.3 \pm 0.3$ ) and free to vary normalizations. We then adopted a bremsstrahlung model having an exponential high-energy cut-off and we obtained a  $\chi^2/\text{dof} = 7/14$  with a plasma temperature of  $13^{+4}_{-3}$  keV, indicative of an exponential decay of the spectrum at high energies. These results imply a factor  $\sim 2$  higher flux (20–100 keV energy band) at the peak of the folded profile ( $1.7 \pm 0.3 \times 10^{-11}$  erg cm<sup>-2</sup> s<sup>-1</sup>) with respect to the phase-averaged flux emission ( $7.1 \pm 1.4 \times 10^{-12}$  erg cm<sup>-2</sup> s<sup>-1</sup>), but undetected variability in the spectral shape.

We studied the pointed *Swift*/XRT spectra in the 0.5–10 keV range, while we used the 0.3–0.7 phase-selected *Swift*/BAT spectrum to provide a coverage of the hard X-ray emission above 15 keV. The BAT spectrum is averaged for many orbital periods and its use in a common fit with the *Swift*/XRT spectra is helpful in giving an estimate of the broad-band spectral shape assuming negligible spectral variability between the pointed and the long-term spectra.

The three *Swift*/XRT spectra showed slightly different spectral shapes and fluxes. We noted that the spectra had the largest discrepancy in the softest part of the X-ray spectrum, and we took it as a possible indication of a varying local column density ( $N_{\text{H}}$ ). Allowing for different values of the neutral absorption for each observation and introducing a multiplicative constant to account for the different fluxes, we obtained a satisfactory account of all the *Swift*/XRT spectra, consistent with a hard power law of best-fitting photon index  $\Gamma = 0.4$ . When the BAT spectrum is added to the fit, the simple power-law model did no longer provide a good fit to the data (reduced  $\chi^2 = 3.0$  for 88 dof), because of the significant steepening in the *Swift*/BAT energy range. The resulting spectrum was much better fitted (reduced  $\chi^2 = 1.15$ , for 87 dof) with a cut-off power-law model (cutoffpl in XSPEC) having a best-fitting photon index  $\Gamma = -0.4 \pm 0.3$  and a cut-off energy  $E_{\text{cut}} = 6.8^{+1.6}_{-1.2}$  keV. Adopting a model with a power law multiplied by a high-energy cut-off with an e-folding energy ( $\text{Exp}[(E_{\text{cut}} - E)/E_{\text{fold}}]$ , highcut model), we obtained a reduced  $\chi^2$  of 1.08 for 86 dof, that provides, however, only a marginal improvement (F-test chance improvement 4.4 per cent) with respect to the cutoffpl model (Fig. 5). In Table 2, we show the best-fitting spectral parameters and error bars calculated at  $\Delta\chi^2 = 2.7$  (90 per cent confidence level) for this final model.

## 5 DISCUSSION

In this paper we presented the first study on the timing and spectral properties of the X-ray source J1944221 exploiting the data recorded by the X-ray instruments on board of *Swift*. The source showed significant and steady higher accretion rates since 2011, and it is clearly resolved in hard X-rays up to  $\sim 45$  keV. The timing analysis on the *Swift*/BAT survey revealed a periodic modulation with a period of  $P_0 = 166.5 \pm 0.5$  d, that we associate to the orbital period of an X-ray binary system. The profile of the light curve folded at  $P_0$  shows a peak in emission lasting  $\sim 1/8$  of the period. The folded

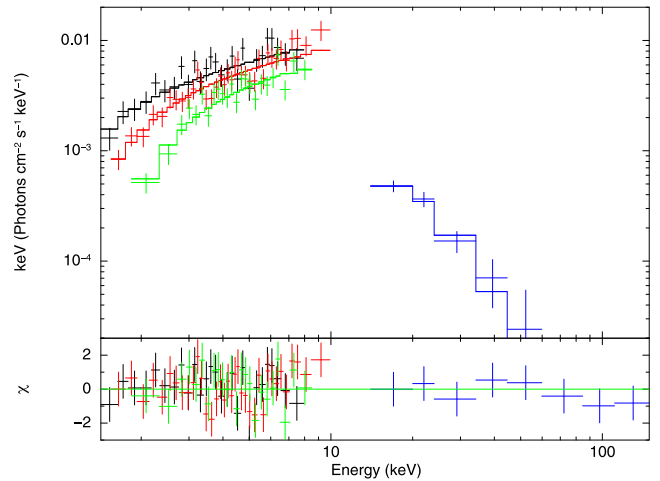


**Figure 5.** Data, best-fitting unfolded model (upper panel), and residuals in units of  $\sigma$  (lower panel) for the combined *Swift*/XRT and *Swift*/BAT spectra, adopting the model of Table 2. Black, red, green, and blue colour for the *Swift*/XRT Obs.ID 01, 02, 03, and *Swift*/BAT data, respectively.

**Table 2.** Best-fitting spectral parameters for the combined *Swift*/XRT and *Swift*/BAT spectra adopting a model of an absorbed power law with a high-energy cut-off. We left the column density of the *Swift*/XRT data sets free to vary, while the column density of the BAT spectrum is tied to the Obs.ID 01 value.

Parameter	Best-fitting value
Common fitting values	
$\Gamma$	$0.4 \pm 0.2$
$E_{\text{cut}}$ (keV)	$18^{+4}_{-10}$
$E_{\text{fold}}$ (keV)	$7.3^{+3}_{-2.7}$
Obs.ID 01	
$N_{\text{H}}$ ( $10^{22}$ cm <sup>-2</sup> )	$0.8 \pm 0.5$
$F_{0.5-10 \text{ keV}}^a$	$10 \pm 1.3$
Obs.ID 02	
$N_{\text{H}}$ ( $10^{22}$ cm <sup>-2</sup> )	$1.7 \pm 0.6$
$F_{0.5-10 \text{ keV}}^a$	$9.0 \pm 0.6$
Obs.ID 03	
$N_{\text{H}}$ ( $10^{22}$ cm <sup>-2</sup> )	$3.7 \pm 1$
$F_{0.5-10 \text{ keV}}^a$	$6.6 \pm 0.6$
BAT	
$C_{\text{BAT}}$	$(8.6^{+20}_{-2.0}) \times 10^{-2}$
$F_{15-100 \text{ keV}}^a$	$2.4 \pm 0.4$
$\chi^2 / \text{dof}$	93/86

Note. <sup>a</sup>In units of  $10^{-11}$  erg cm<sup>-2</sup> s<sup>-1</sup>

profile is consistent with a scenario of enhanced accretion from a compact object close to the periastron passage, as typical for the class of Be X-ray binary systems. Our interpretation agrees with Masetti et al. (2012), that on the base of the presence of strong H  $\alpha$  line in the optical spectrum, first proposed a high-mass X-ray identification for the J194221.

We analysed the broad-band X-ray spectrum of J194221 using the XRT pointed observation data in the soft X-ray band and the BAT survey data. The spectrum can be well modelled with a

<sup>7</sup> <http://swift.gsfc.nasa.gov/docs/heasarc/caldb/swift/>

hard ( $\Gamma = 0.4$ ) absorbed power law with an energy cut-off  $E_{\text{cut}}$  at  $\sim 18$  keV and a folding energy  $E_{\text{fold}} \sim 7.3$  keV. We found evidence of a possible varying local neutral absorber in the *Swift*/XRT spectra. Among the three examined observations, the lowest column density value is consistent with the Galactic value in the direction of the source ( $1.09 \times 10^{22} \text{ cm}^{-2}$ ; Dickey & Lockman 1990), while the highest value indicates moderate local absorption. The hard X-ray spectrum, the high-energy folding and cut-off energies, and the variations in the equivalent hydrogen column observed in close (within few days) observations at the putative periastron passage are all typical spectral characteristics of the Be X-ray binary class and further support our identification of the source as an active Be X-ray binary (see also for similar interpretations Cusumano et al. 2013; La Parola et al. 2013, 2014).

#### ACKNOWLEDGEMENTS

This research has made use of data and/or software provided by the High Energy Astrophysics Science Archive Research Center (HEASARC), which is a service of the Astrophysics Science Division at NASA/GSFC and the High Energy Astrophysics Division of the Smithsonian Astrophysical Observatory. This work has been supported by ASI grant I/011/07/0.

#### REFERENCES

- Chenevez J. et al., 2011, *Astron. Telegram*, 3816, 1  
 Cusumano G., La Parola V., Romano P., Segreto A., Vercellone S., Chincarini G., 2010, *MNRAS*, 406, L16  
 Cusumano G., Segreto A., La Parola V., Masetti N., D’Aì A., Tagliaferri G., 2013, *MNRAS*, 436, L74  
 D’Aì A., La Parola V., Cusumano G., Segreto A., Romano P., Vercellone S., Robba N. R., 2011, *A&A*, 529, A30  
 Dickey J. M., Lockman F. J., 1990, *ARA&A*, 28, 215  
 Evans P. A. et al., 2014, *ApJS*, 210, 8  
 Goad M. R. et al., 2007, *A&A*, 476, 1401  
 La Parola V., Cusumano G., Segreto A., D’Aì A., Masetti N., D’Elia V., 2013, *ApJ*, 775, L24  
 La Parola V., Segreto A., Cusumano G., Masetti N., D’Aì A., Melandri A., 2014, *MNRAS*, 445, L119  
 Masetti N., Landi R., Parisi P., Bazzano A., Bird A. J., 2012, *Astron Telegram*, 4209, 1  
 Segreto A., Cusumano G., Ferrigno C., La Parola V., Mangano V., Mineo T., Romano P., 2010, *A&A*, 510, A47  
 Sidoli L. et al., 2011, *Astron Telegram*, 3818, 1

This paper has been typeset from a  $\text{\TeX}/\text{\LaTeX}$  file prepared by the author.